From Simple to Complex Reactions:

Nuclear Collisions near the Coulomb Barrier

K. E. Rehm

Physics Division, Argonne National Lab., Argonne, Illinois 60439, USA

1. Introduction

Collisions between two heavy nuclei produce a diverse spectrum of reaction modes which is much wider than that observed in light ion studies. For the latter case, two processes are observed: direct reactions and compound nucleus formation. Heavy ion reaction studies on the other hand have identified additional processes such as deep-inelastic scattering, incomplete fusion and quasi-fission reactions. While the boundaries between the various processes are usually not well defined, it is generally accepted that with increasing overlap of the two nuclei the interaction evolves from distant collisions where only elastic scattering and Coulomb excitation processes occur, through grazing-type collisions associated with quasi-elastic reactions to deep-inelastic and fusion-fission processes requiring a substantial nuclear overlap. Varying the bombarding energy is a convenient way to change the overlap of the two nuclei. Measurements of excitation functions can thus probe the onset and the interplay of the various reaction modes. Experiments at bombarding energies in the vicinity of the Coulomb barrier are particularly suited for comparisons with theoretical predictions since the small number of degrees of freedom involved in the interaction greatly simplifies the calculations.

In the first part of this contribution a short overview is given on the status of heavy ion reaction studies at energies in the vicinity of the Coulomb barrier. In the second part two experiments, one involving simple and the other studying complex reactions, are discussed in more detail.

2. Heavy Ion Reaction Modes at Energies Close to the Coulomb Barrier

2.1 Elastic and Inelastic Scattering

One of the most noticeable differences between heavy-ion and light-ion induced reactions is the strong increase of the reaction yields for heavy-ion collisions. Figure 1 demonstrates this for angular distributions of elastic and inelastic scattering populating the lowest excited state measured with ^{16}O,^{28}Si,^{58}Ni and ^{86}Kr projectiles on ^{208}Pb[1-4]. The solid lines are the results of distorted-wave Born approximation (DWBA) or coupled-channel (CC) calculations using measured B(EL) values. They describe the shape and the absolute magnitude of the distributions remarkably well. The cross hatched bars represent the angle-integrated inelastic yields which show a strong increase from 23 mb for ^{16}O to 1770 mb for ^{86}Kr. This strong increase in the inelastic-scattering yield is caused mainly by the Z^2 dependence of the Coulomb

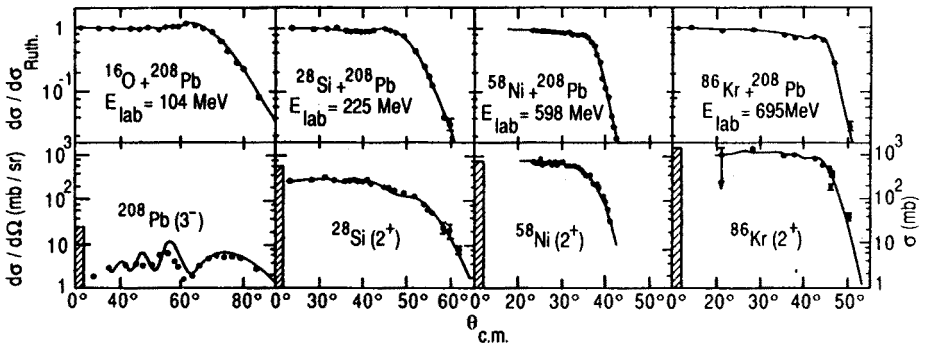

Fig. 1. Angular distributions for elastic scattering and inelastic excitation of the lowest state measured with ^{16}O, ^{28}Si, ^{58}Ni and ^{86}Kr projectiles on ^{208}Pb. The solid lines are the results of DWBA or coupled-channel calculations. The cross hatched bars represent the angle-integrated cross sections.

excitation cross sections. The large yields for inelastic scattering can have a substantial influence on the elastic channel as seen e.g. for the case of ^{86}Kr + ^{208}Pb. For these systems elastic scattering can not be described using an Optical Model calculation. The elastic channel must be included as a separate channel in a CC calculation in order to describe the deviations from Rutherford scattering observed already at small scattering angles.

2.2 Quasi-elastic Transfer Reactions

While the strong rise in the inelastic scattering yields is expected because of the increased Coulomb excitation probability, quasi-elastic transfer reactions which require a larger overlap of the two colliding nuclei also exhibit increased yields for heavier systems. Figure 2 shows the contributions of quasi-elastic transfer reactions to the total reaction yields for ^{16}O[5,6] and ^{58}Ni[7,8] induced reactions on $^{120,122}Sn$ and ^{208}Pb, respectively, measured at energies about 25% above the Coulomb barrier. As can be seen from Figure 2 the contributions of the quasi-elastic transfer reactions to the total reaction yield change considerably with increasing mass of the system. While the systems ^{16}O + ^{122}Sn and ^{16}O + ^{208}Pb are still dominated by fusion processes (shown as cross-hatched bars in Figure 2) fusion (which includes compound-nucleus formation and fission) is less important for the heavier systems, where transfer reactions are the dominant reaction modes.

The various reactions contributing to the quasi-elastic transfer yields for the system ^{48}Ti + ^{208}Pb are shown in Figure 3[9]. Similar to the results of many other systems neutron-transfer processes, in particular the one-neutron pickup reaction (^{48}Ti,^{49}Ti), dominate the quasi-elastic cross sections. Other one-particle transfers show smaller yields. The angular distributions for the energy-integrated transfer reactions are generally bell shaped. Figure 4 illustrates this feature for various neutron transfer reactions induced by Ti, Ni and Se ions on ^{208}Pb[10]. The width of the distributions decreases in going from ^{48}Ti

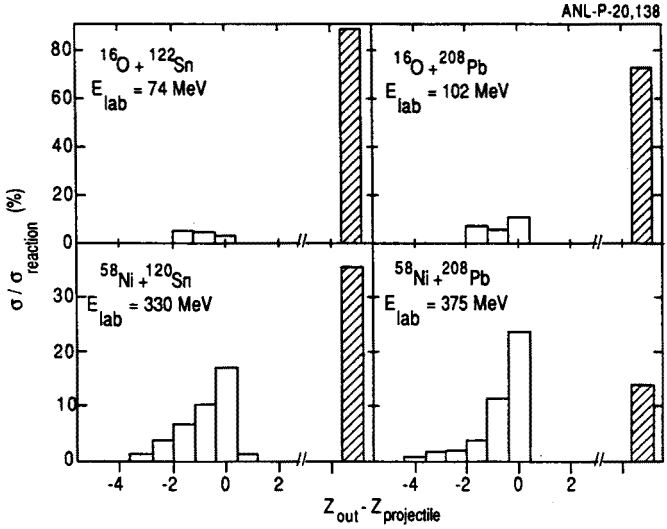

Fig. 2. Contributions of quasi-elastic (open bars) and fusion reactions (cross-hatched bars) to the total reaction cross sections for ^{16}O and ^{58}Ni-induced reactions on $^{120,122}Sn$ and ^{208}Pb. The beam energies are indicated in the figure.

to ^{80}Se. If the cross section $d\sigma/d\Omega$ is transformed into $d\sigma/dR$, however, where R is the distance of closest approach for a given scattering angle θ and plotted as a function of the reduced radius parameter $d_o = R/(A_1^{1/3} + A_2^{1/3})$ it becomes clear that all neutron-transfer reactions in this mass range occur with maximum probability at an internuclear distance corresponding to a radius parameter $d_o = 1.5$ fm. Theoretical calculations within the framework of DWBA are able to reproduce the measured angular distributions. Figure 5 shows as an example the angular distributions for the one-particle transfer reactions $^{40}Ca(^{28}Si,^{27}Si)^{41}Ca$ and $^{40}Ca(^{28}Si,^{27}Al)^{41}Sc$ populating various levels in the mass 27 and 41 nuclei[11]. With the exception of a slight shift of the theoretical angular distribution towards larger angles, one-step DWBA calculations predict the shape and the absolute magnitude for both reactions within a factor of 2.

2.3 Multi-particle Transfer Reactions

While the simplest quasi-elastic reaction processes - inelastic scattering and one-nucleon transfer reactions - are quite well reproduced within current theoretical models, multi-particle transfers are still lacking a satisfactory theoretical explanation. It is well known from a variety of earlier studies that two-particle transfer reactions exhibit yields which are larger by factors of 10^2 to 10^3 than those calculated within the framework of the one-step DWBA[12]. Inclusion of multi-step processes which are quite strong at energies close to the Coulomb barrier results in a better agreement with the data[13] but a complete microscopic description of the multi-particle transfer reactions has not yet been achieved. The number of multi-particle transfer reactions

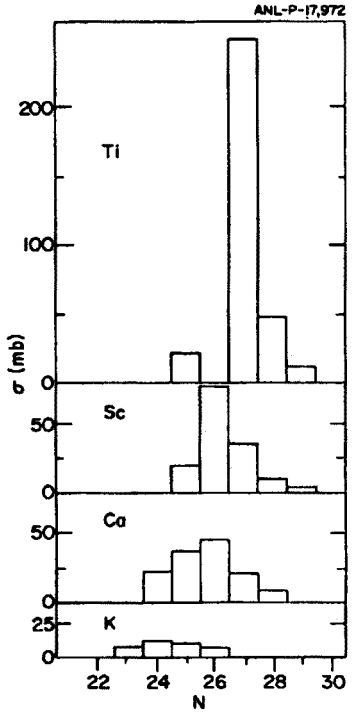

Fig. 3. Energy- and angle-integrated cross sections for the strongest transfer reactions in the system ^{48}Ti + ^{208}Pb at E_{lab}=300 MeV.

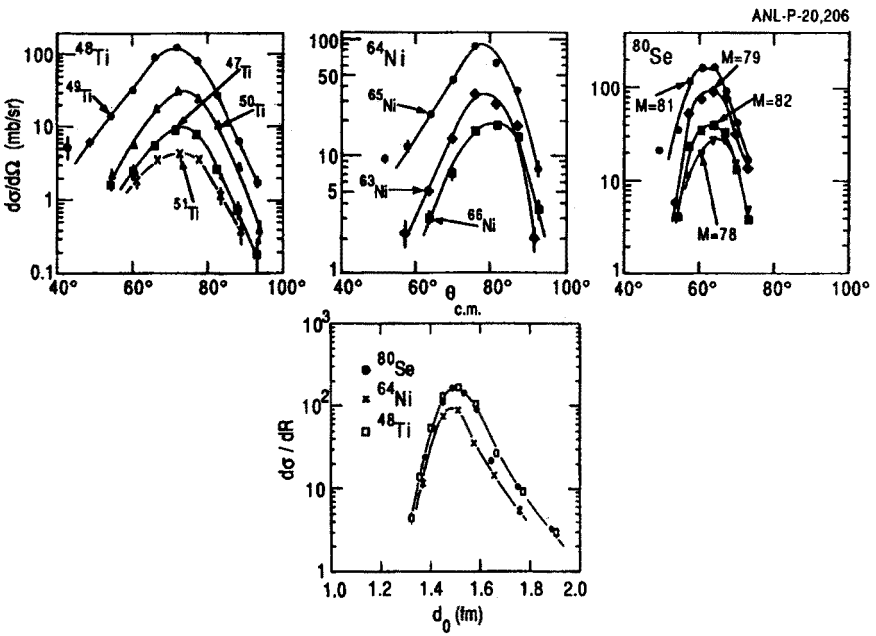

Fig. 4. Angular distributions for the energy-integrated neutron transfer reactions induced by ^{48}Ti, ^{64}Ni and ^{80}Se projectiles on ^{208}Pb at 300, 380 and 525 MeV, respectively. The solid lines serve to guide the eye.

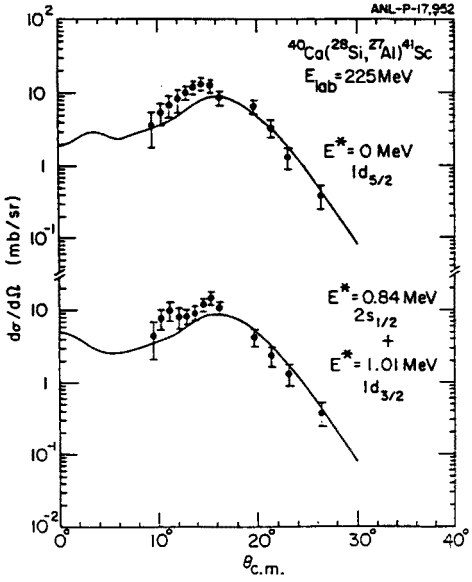

Fig. 5. Angular distributions for the one-particle transfer reactions $^{40}Ca(^{28}Si,^{27}Si)^{41}Ca$ and $^{40}Ca(^{28}Si,^{27}Al)^{41}Sc$ populating various levels in the mass 27 and 41 nuclei. The solid lines are the result of DWBA calculations.

accessible in heavy-ion collisions is considerable as can be seen from Figure 6 showing energy spectra for the strongest reaction channels

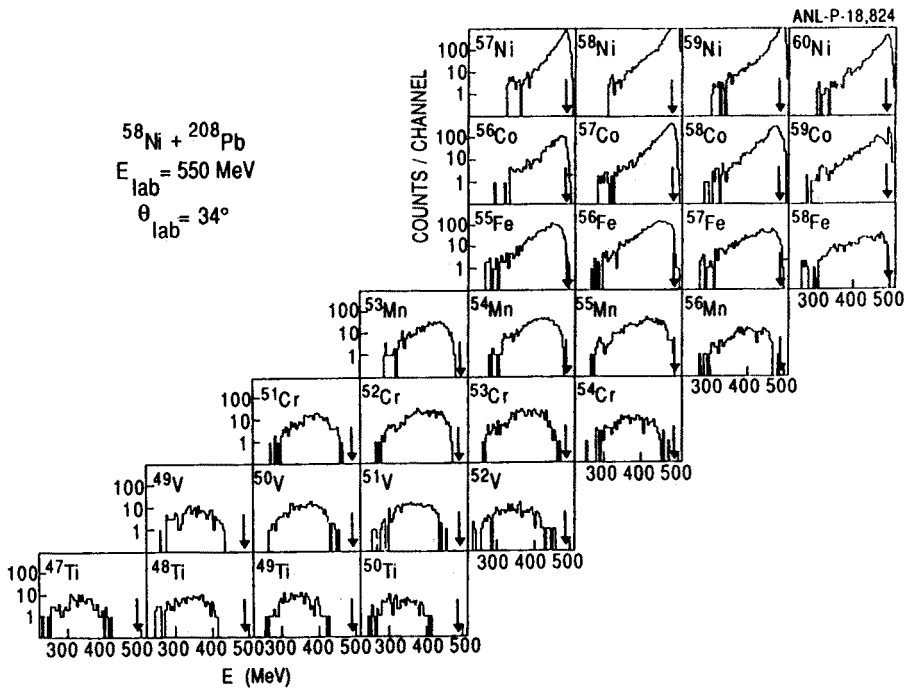

Fig. 6. Energy spectra for the strongest reaction channels in the system $^{58}Ni + ^{208}Pb$ at E_{lab}=550 MeV and θ_{lab}=34°. The arrows correspond to Q=0.

in the system ^{58}Ni + ^{208}Pb at E_{lab}=550 MeV[14]. The importance of these complex transfers increases at higher bombarding energies. The multi-particle transfer reactions are also associated with more negative Q-values and constitute the dominant contribution to the deep-inelastic reaction mode. The angular distributions of these processes change from bell-shaped structures to more forward peaked distributions especially at higher bombarding energies. This is exhibited in the Wilczyński plots[15] (i.e. contours of constant cross section $d\sigma/d\theta$ in a Q-value vs. scattering-angle plane) for the system ^{58}Ni + ^{208}Pb at 345 and 375 MeV in Figure 7. Several observations can be made from Figure 7:

ANL-P-20,851

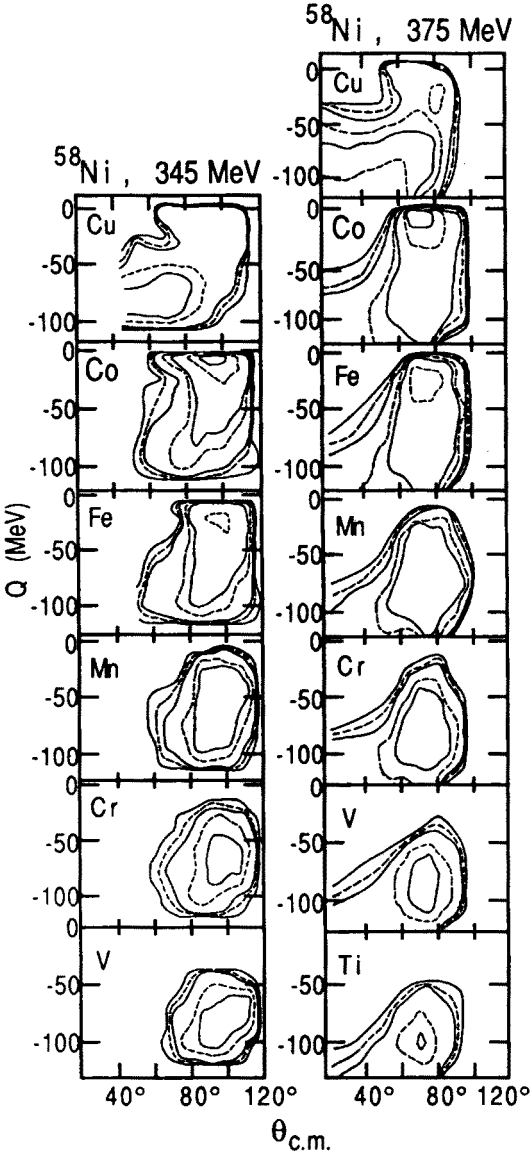

Fig. 7. Wilczyński-plots (contour lines of constant cross sections in a Q-value - angle plane) for various elements measured in the system ^{58}Ni + ^{208}Pb at 345 and 375 MeV, respectively. The outermost solid contour line corresponds to a cross section of 10 μb/(rad MeV) with an increase by a factor of 10 for each subsequent solid line.

(i) All reaction channels observed in this system contain some yields associated with very negative Q-values (deep-inelastic reactions).

(ii) Processes with Q=0 can only be found for few-nucleon transfer reactions. (See also Ref.[9] for Wilczyński plots for individual isotopes including the neutron-transfer channels.)

(iii) There is no clear distinction between processes involving small and large energy transfers (quasi- and deep-inelastic reactions). Deep-inelastic processes seem to evolve gradually from quasi-elastic reactions.

(iv) Deep-inelastic reactions are present even at low bombarding energies, although the typical characteristics (forward peaking of the angular distributions) develop only at energies above the Coulomb barrier.

2.4 Fusion Reactions

The formation of a compound nucleus is the process requiring the largest internuclear overlap. While for light-ion reactions at energies above the Coulomb barrier fusion is generally the strongest reaction mode the large angular momenta associated with heavy-ion reactions lead to a reduction of the fusion probability. At subbarrier energies, however, heavy-ion induced fusion experiments performed during the past 10 years showed an unexpected enhancement of the fusion yields when compared to one-dimensional barrier penetration calculations[16-18]. In addition a strong nuclear-structure dependence of the fusion cross section has been observed particularly in systems involving ^{58}Ni and ^{64}Ni nuclei. Various theoretical explanations have been developed in order to explain these observations[16-18]. The coupling of other reaction channels and additional degrees of freedom (e.g. neck formation) have been invoked in order to obtain a quantitative understanding of the large enhancement factors. The reaction channels which in a coupled-channel treatment have the dominant contributions can be deduced from Figure 8 showing the energy dependence of fusion, deep-inelastic scattering, quasi-elastic

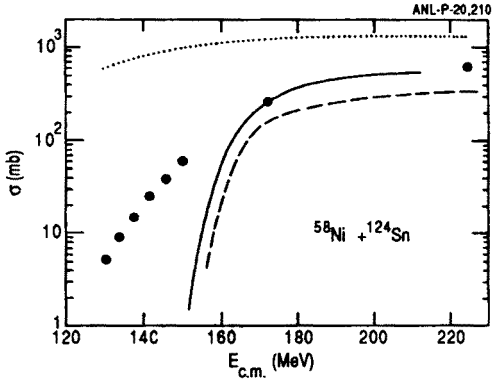

Fig. 8. Energy dependence of fusion (solid line), deep-inelastic (dashed line), quasi-elastic transfer reactions (circles) and inelastic scattering (dotted line) of the lowest 2^+ and 3^- states measured for the system ^{58}Ni + ^{124}Sn.

transfer and inelastic scattering measured for the system ^{58}Ni + ^{124}Sn[10]. At energies in the vicinity of the Coulomb barrier inelastic excitation and quasi-elastic transfer processes (dominated by neutron-transfer reactions) are the most important reaction channels. Detailed CC calculations have been quite successful in explaining the large subbarrier enhancement factors, particularly for lighter systems[19].

In the following two experiments related to peripheral (Section 3) and central collisions (Section 4) will be discussed in more detail.

3. Neutron Transfer at Large Distances

Nucleon transfer at large internuclear distances is usually described within a semiclassical tunneling picture with the two interacting nuclei moving on classical Rutherford trajectories. In a plot of cross section vs. distance of closest approach the transfer cross sections exhibit exponential falloffs towards larger distances with slope parameters which are determined by the binding energy of the transferred particle via the equation

$$2\alpha = 2\sqrt{2E_b m_n} \qquad (1)$$

In eq. (1) E_b is the neutron binding energy and m_n the reduced mass of the transferred nucleon.

For the majority of the experiments good agreement between the expected slope parameter and the experimental results has been observed[20].

Several recent experiments[21], however, have revealed deviations from the simple tunneling picture. Most of the discrepancies are observed for two-neutron transfer reactions which, because of the increased mass transfer and the larger binding energy, should exhibit a slope parameter which is about twice as steep as the one observed for the one-neutron transfer case. Experimentally, however, the falloff for two-neutron transfer reactions is found to be similar to that for one-neutron transfer. This is shown for the one- and two-neutron transfer reactions (^{58}Ni,^{59}Ni) and (^{58}Ni,^{60}Ni) on ^{232}Th in Figure 9 where the quantity

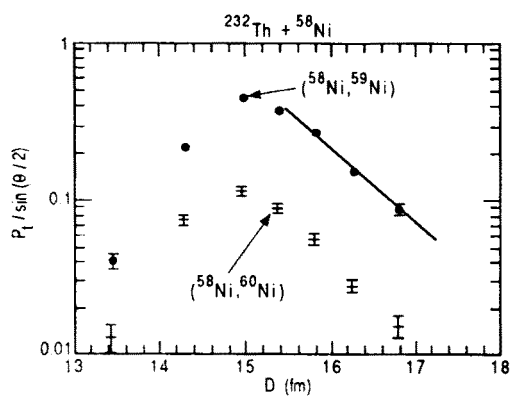

Fig. 9. Transfer probability $P_t/\sin(\theta/2)$ plotted as function of the distance of closest approach D for the one- and two-neutron transfer reactions (^{58}Ni,^{59}Ni) and (^{58}Ni,^{60}Ni) on ^{232}Th at E_{lab}=500 MeV. The solid line for the one-neutron transfer reaction corresponds to a slope parameter calculated with eq. (1).

$P_t/\sin(\theta/2)$ is plotted vs the distance of closest approach D. The transfer probability P_t is defined as the ratio between the transfer- and the Rutherford cross sections.

$$P_t = d\sigma_{tr}/d\sigma_{Rutherford} \quad (2)$$

The solid line in Figure 9 for the (^{58}Ni,^{59}Ni) reaction is obtained from eq. (1). As can be seen the falloff towards larger radii is very similar for one- and two-neutron transfer reactions. A comparison of the experimental and the theoretical slope parameters calculated using eq. (1) for ^{58}Ni induced one- and two-neutron transfer reactions on various target nuclei with mass A is given in Figure 10. For the one-neutron transfer reactions good agreement between experiment and theory is observed while for the majority of the two-neutron transfer cases smaller decay constants are obtained. The few examples where the correct slope parameter has been observed were measured at energies very close to the Coulomb barrier. The dependence of the slope parameter on the bombarding energy is illustrated in Figure 11 for the one- and two-neutron transfer reaction measured in the system ^{58}Ni + ^{208}Pb. The correct slope parameter is observed only at energies in the immediate vicinity of the Coulomb barrier V_c. At higher bombarding energies the slope parameter approaches values measured for one-neutron transfer reactions. The results for one-neutron transfer reactions on the other hand are in reasonable agreement with the theoretical expectations over the entire energy range (see top part of Figure 11).

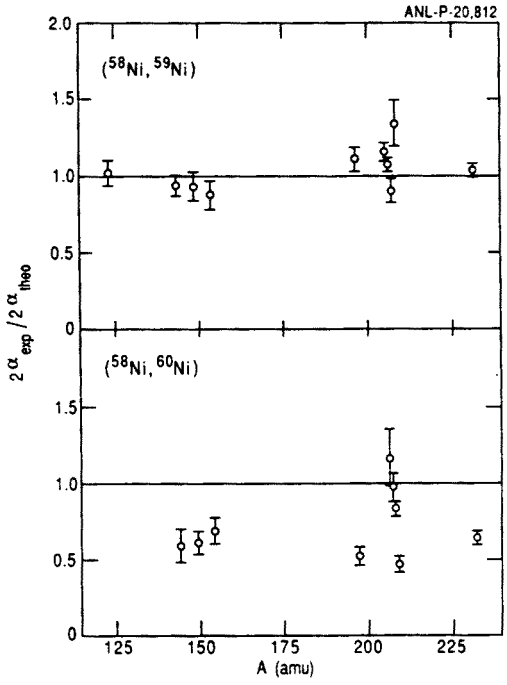

Fig. 10. (top): Ratios of the experimental slope parameters $2\alpha_{exp}$ and the theoretical values for the one-neutron pickup reaction (^{58}Ni,^{59}Ni) on various nuclei with mass A. (bottom): Same as (top) but for the two-neutron transfer reaction (^{58}Ni,^{60}Ni).

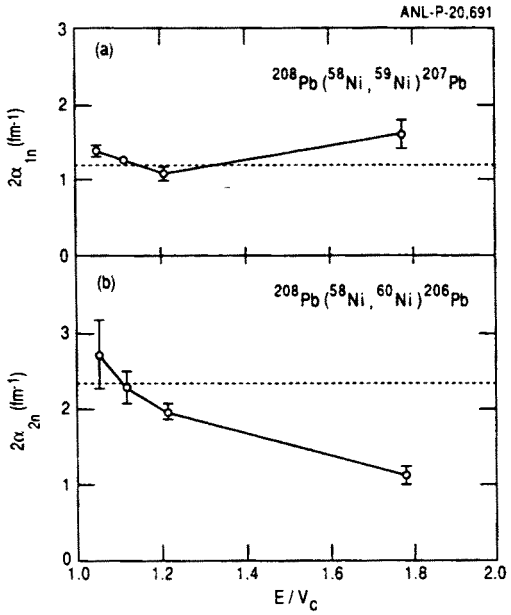

Fig. 11. (top): Experimental slope parameter $2\alpha_{exp}$ for the one-neutron transfer reaction $^{208}Pb(^{58}Ni,^{59}Ni)^{207}Pb$ as function of the energy above the Coulomb barrier E/V_c. The dotted line is the theoretical slope calculated from eq. (1).
(bottom): Same as (top) but for the two-neutron transfer reaction $^{208}Pb(^{58}Ni,^{60}Ni)^{206}Pb$.

In order to gain a better understanding of this energy dependence the questions regarding the applicability of the semiclassical model need to be investigated. It is known from transfer reaction studies involving lighter ions that the partial-wave distribution associated with two-particle transfer reactions is much more localized than in the one-particle transfer case. As shown e.g. in Ref [22,23] a treatment of the scattering process within classical dynamics, i.e. involving Rutherford trajectories, requires that the width of the partial wave distribution is larger than a critical value Δl_c given by

$$\Delta \ell_c = \frac{\sqrt{\eta}}{\sin(\theta_0/2)} \tag{3}$$

In eq. (3), η is the Sommerfeld parameter and θ_0 the scattering angle associated with the maximum of the angular distribution.

Δl_c can be transformed into a limit for the width of the form factor ΔD_c:

$$\Delta D_c = \sqrt{\hbar D_0 \sqrt{\frac{2}{\mu V_c}} \frac{\left(\frac{E}{V_c} - 1\right)}{\sqrt{\frac{E}{V_c}}}} \tag{4}$$

where D_0 is the distance of closest approach, μ the reduced mass and V_c the Coulomb barrier.

The requirements for a semiclassical treatment are that the width of the l-distribution (or the form factor) is larger than the critical values given by eqs. (3,4). Reaction processes involving very localized form factors have to be treated as quantal diffraction processes and the use of classical trajectories is not justified. As can be seen from eq. (4) the requirement of $\Delta D > \Delta D_c$ is easily fulfilled for energies in the vicinity of the Coulomb barrier where ΔD_c approaches zero. This explains the experimental results that at low bombarding energies the theoretical slope parameters are obtained. With increasing energy the critical width ΔD_c increases. Reactions with localized form factors such as two-particle transfer reactions exceed the requirement $\Delta D > \Delta D_c$ already at relatively low bombarding energies and thus have to be treated as diffractional processes. The fact that a localized form factor can result in a similar distribution for $P_t/\sin(\theta/2)$ is emphasized in Figure 12 for the case of ^{58}Ni induced transfer reactions on ^{232}Th. The solid

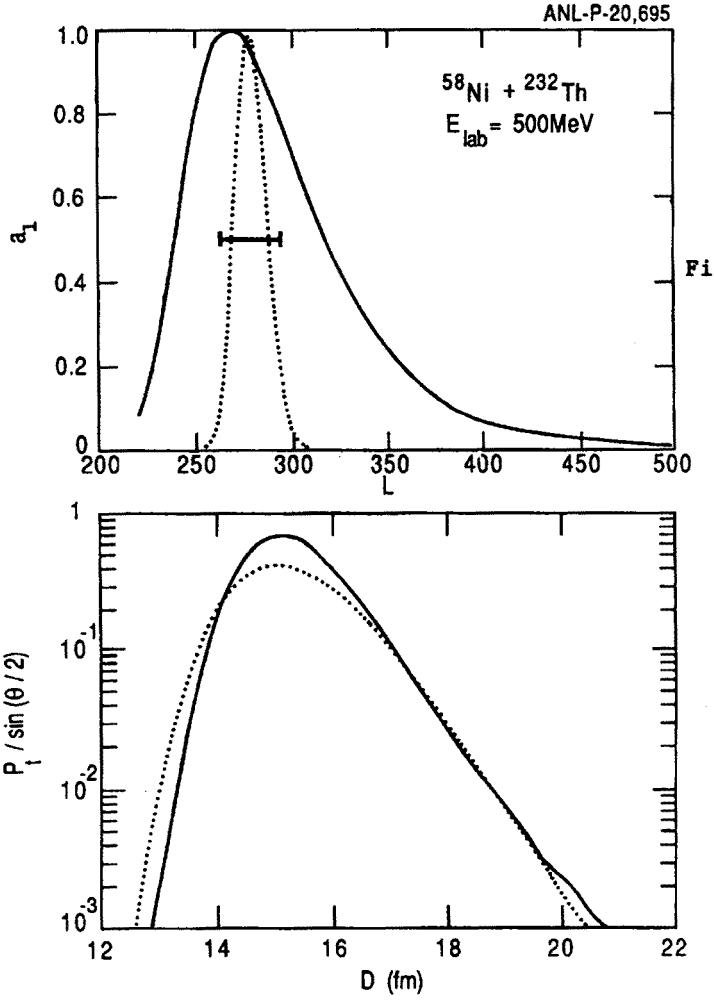

Fig. 12. Form factors (top) and the resulting transfer probabilities (bottom) calculated using eq. (5) for the system ^{58}Ni + ^{232}Th at E_{lab}=500 MeV.

line in Figure 12 for the l-distribution (top) was obtained from a DWBA calculation for the one-neutron transfer reaction $^{232}Th(^{58}Ni,^{59}Ni)^{231}Th$. The resulting transfer probability calculated from the expression for the cross section

$$\frac{d\sigma}{d\Omega} = \left| \frac{1}{2ik} \sum_{\ell} (2\ell + 1) a_{\ell} e^{2i\sigma_{\ell}} P_{\ell}(\cos\theta) \right|^2 \qquad (5)$$

is shown as a solid line in the lower part of Figure 12. The dotted line in Figure 12 shows that a transfer probability with a similar slope can be obtained with a very localized form factor which is smaller than the critical value ΔD_c indicated by the solid bar in Figure 12.

These results emphasize that data of neutron transfer reactions at large internuclear distances have to be investigated with caution. In many cases bombarding energies and scattering angles have been used where the assumptions of pure Rutherford trajectories are no longer justified. Furthermore for data obtained at higher bombarding energies the question of the applicability of the semiclassical model has to be investigated very carefully. If the width of the form factor involved in the transfer reaction is small the assumption of classical trajectories is no longer justified and the analysis must be performed within a diffraction model.

4. Measurements of Heavy-Ion Induced Fusion Reactions using a New Technique

The enhancement of heavy-ion induced fusion reactions has been one of the most discussed phenomena in low-energy heavy-ion physics during the last decade[16-18]. The surprising dependence of the fusion probability on details of the underlying nuclear structure in many systems (e.g. Ni + Ni, S + Ni, S + Mo) has found its explanation in the coupling of strong quasi-elastic reaction channels (inelastic scattering and few-nucleon transfers) to the elastic channel which, in a two-state approximation, adds an additional term to the interaction energy and therefore leads to an energy gain enhancing the fusion probability at low energies[24]. Many of the results obtained for lighter systems are well reproduced by coupled-channel calculations. Heavier systems, however, still show discrepancies with theoretical predictions which are presently hard to understand. More systematic investigations of medium mass and heavy systems are needed in order to study the influence of nuclear structure on the fusion process in more detail. These experiments are quite difficult because the separation of the evaporation residues (ER's) from the incident beam at forward angles becomes more difficult for heavier systems. Various techniques have been used to achieve this separation:

1. Detection of the recoiling nuclei using velocity filters or electrostatic separators.

2. Measurement of characteristic X-rays of the ER's.

3. Measurements of characteristic γ-lines of the ER's.

The determination of absolute cross sections using these techniques, however, requires a detailed knowledge of the charge distributions or the γ-decay schemes of the residual nuclei. We have started to use the method of a gas-filled magnet[25-29] for the detection of ER's produced in subbarrier fusion reactions.

In a magnet the trajectory of a charged particle with mass m, nuclear charge Z and atomic charge state q is given by its magnetic rigidity

$$B\rho = mv/q. \tag{6}$$

If the magnet is filled with gas the velocity v and the charge state q in eq. (6) will be replaced by their average values $\bar{v}$ and $\bar{q}$ with

$$\bar{q} \sim \bar{v}\, Z^{\gamma} . \tag{7}$$

The exponent γ depends on the mass of the particle and the properties of the gas and is typically between 0.3 and 0.6. Combining eq. (6) and (7) one obtains the averaged magnetic rigidity

$$B\bar{\rho} \sim m/Z^{\gamma} , \tag{8}$$

which is now independent of the velocity v. Calculations using more detailed expressions for the charge state distributions[29] show in addition a dependence on the bombarding energy, but the general features of eq. (8) are preserved. For the system ^{64}Ni + ^{100}Mo eq. (8) predicts a larger rigidity for the ER's than for the elastically scattered particles. Since in addition the time-of-flight (TOF) through the magnet is considerably larger for the heavier ER's a simultaneous measurement of $B\rho$ and TOF results in a clear separation of the ER's from the elastically scattered particles. Figure 13 shows two-dimensional plots of TOF vs. $B\rho$ measured with a gas-filled Enge Split Pole Spectrograph for the system ^{64}Ni + ^{100}Mo. As can be seen the ER's are clearly separated from the much more intense ^{64}Ni particles even at scattering angles as small as 1.2°. Since the magnetic field can be chosen such that the majority of the elastically scattered particles do not enter the detector high beam currents can be used in the experiment. First experiments for the ^{64}Ni + ^{100}Mo system confirmed the strong subbarrier fusion enhancement which can not be explained by current coupled-channel calculations[30].

5. Conclusions

The last 10 years have witnessed a significant increase in the number of experimental and theoretical studies of heavy-ion collisions at energies near the Coulomb barrier. A variety of questions have been answered but many problems still remain. For inelastic scattering experiment and theory are usually in good agreement. One-neutron transfer reactions are also well described by one-step DWBA calculations, although the quality of the data is in most cases not sufficient to rule out the influence of more complicated multistep processes. Many areas have barely been touched in high resolution heavy-ion experiments. The transition from simple one-step to complex multiparticle transfer reactions has not been investigated in detail, neither experimentally nor theoretically.

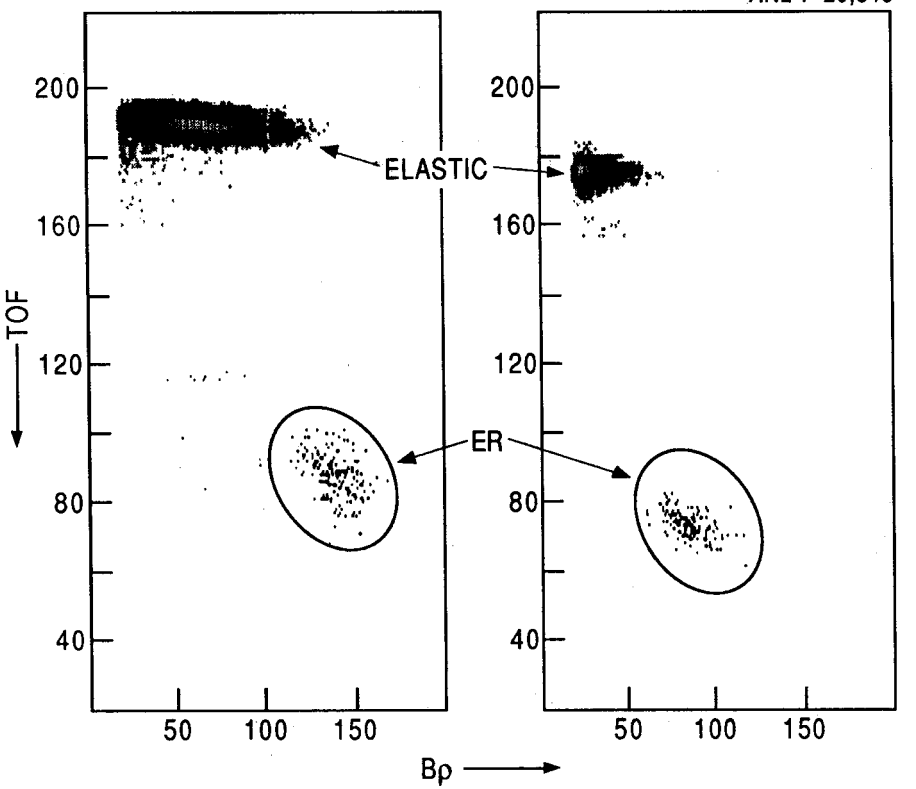

Fig. 13. Two-dimensional plots of TOF vs. magnetic rigidity Bρ, measured for the system ^{64}Ni + ^{100}Mo using the gas-filled magnet technique. Evaporation residues and elastically scattered particles are clearly separated. The bombarding energies and scattering angles are 248.7 MeV and 3° (left) and 217.2 MeV and 1.2° (right), respectively.

The main difference between heavy-ion induced reactions and light-ion collisions is the increased importance of the couplings between the different reaction modes. As a result of this coupling, reaction modes associated with central collisions, such as fusion, can be influenced by peripheral reactions. These processes (inelastic scattering and few-nucleon transfers) depend through their BE(L) values and spectroscopic factors strongly on the structure of the interacting nuclei. Fusion reactions which were once thought to be mainly a macroscopic processes become through channel coupling strongly dependent on nuclear structure effects. Similar effects must also be present for deep-inelastic collisions but have not been studied so far.

6. Acknowledgement

The results presented in this contribution have been obtained in collaboration with B. Glagola, D. Henderson, J. Gehring, W. Kutschera, F. L. H. Wolfs and A. Wuosmaa. This work was supported by the Department of Energy, Nuclear Physics Division, under contract W-31-109-ENG-38.

References

[1] F.D. Becchetti et al., Phys. Rev. C6, 2215 (1972).
[2] J.J. Kolata et al., Phys. Rev. C30, 125 (1984).
[3] M. Beckermann et al., Phys. Rev. C36, 657 (1987).
[4] J. Cheng-Lie et al., Phys. Rev. Lett. 47, 1039 (1981).
[5] H. Spieler et al., Z. Phys. A278, 241 (1976).
[6] F. Videbaek et al., Phys. Rev. C15, 954 (1977).
[7] A.M. van den Berg et al., Phys. Rev. C37, 178 (1988).
[8] K.E. Rehm et al., Phys. Rev. C42, 2497 (1990).
[9] K.E. Rehm et al., Phys. Rev. C37, 2629 (1988).
[10] K.E. Rehm, Annu. Rev. Nucl. Part. Sci. 41, 429 (1991).
[11] M.F. Vineyard et al., Phys. Rev. C33, 1325 (1986).
[12] P.P. Tung et al., Phys. Rev. C18, 1663 (1978).
[13] C.A. Ogilvie et al., Phys. Rev. C39, 139 (1989).
[14] K.E. Rehm et al., to be published.
[15] J. Wilczyński, Phys. Lett. B47, 484 (1973).
[16] M. Beckermann, Phys. Lett. C129, 145 (1985).
[17] S.G. Steadman and M.J. Rhoades-Brown, Annu. Rev. Nucl. Part. Sci. 36, 649 (1986).
[18] M. Beckermann, Rep. Prog. Phys. 51, 1047 (1988).
[19] H. Esbensen and S. Landowne, Nucl. Phys. A492, 473 (1989).
[20] W. von Oertzen, Proc. Workshop on the Interface between Nuclear Structure and Heavy Ion Reaction Dynamics, Notre Dame, Indiana 1990, Institute of Physics Conference Series 109, Bristol 1991 and references therein.
[21] K.E. Rehm et al., submitted to Phys. Rev. C.
[22] P.J. Siemens and F.D. Becchetti, Phys. Lett. B42, 389 (1972).
[23] V.M. Strutinski, Phys. Lett. B44, 245 (1973).
[24] C.H. Dasso et al. Nucl. Phys. A405, 381 (1983).
[25] C.B. Fulmer and B.L. Cohen, Phys. Rev. 109, 94 (1958).
[26] P. Armbruster, Nukleonik 3, 188 (1961).
[27] H. Miyatake et al., Nucl. Instr. and Meth. B26, 309 (1987).
[28] A. Ghiorso et al., Nucl. Instr. and Meth. A269, 192 (1988).
[29] M. Paul et al., Nucl. Instr. and Meth. A277, 418 (1989).
[30] M.L. Halbert et al., Phys. Rev. C40, 2558 (1989).